AFRL-RV-PS-
TR-2017-0169

ARRAYS OF SYNTHETIC ATOMS: NANOCAPACITOR BATTERIES WITH LARGE ENERGY DENSITY AND SMALL LEAK CURRENTS

Alfred Hubler

University of Illinois at Urbana-Champaign
1110 W. Green Street
Urbana, IL 61801

28 Nov 2017

Final Report

AIR FORCE RESEARCH LABORATORY
Space Vehicles Directorate
3550 Aberdeen Ave SE
AIR FORCE MATERIEL COMMAND
KIRTLAND AIR FORCE BASE, NM 87117-5776

DTIC COPY

NOTICE AND SIGNATURE PAGE

This report is the result of contracted fundamental research which is exempt from public affairs security and policy review in accordance with AFI 61-201, paragraph 2.3.5.1. This report is available to the general public, including foreign nationals. Copies may be obtained from the Defense Technical Information Center (DTIC) (http://www.dtic.mil).

AFRL-RV-PS-TR-2017-0169 HAS BEEN REVIEWED AND IS APPROVED FOR PUBLICATION IN ACCORDANCE WITH ASSIGNED DISTRIBUTION STATEMENT.

//SIGNED//
JESSICA BUCKNER
Program Manager

//SIGNED//
PAUL HAUSGEN, Ph.D.
Technical Advisor, Spacecraft Component Technology

//SIGNED//
JOHN BEAUCHEMIN
Chief Engineer, Spacecraft Technology Division
Space Vehicles Directorate

This report is published in the interest of scientific and technical information exchange, and its publication does not constitute the Government's approval or disapproval of its ideas or findings.

Approved for public release; distribution is unlimited.

REPORT DOCUMENTATION PAGE

Form Approved
OMB No. 0704-0188

1. REPORT DATE *(DD-MM-YYYY)*	2. REPORT TYPE	3. DATES COVERED *(From - To)*
28-11-2017	Final Report	23 Sep 2014 – 25 Sep 2017

4. TITLE AND SUBTITLE

Arrays of Synthetic Atoms: Nanocapacitor Batteries with Large Energy Density and Small Leak Currents

5a. CONTRACT NUMBER
FA9453-14-1-0247

5b. GRANT NUMBER

5c. PROGRAM ELEMENT NUMBER
62601F

6. AUTHOR(S)

Alfred Hubler

5d. PROJECT NUMBER
8809

5e. TASK NUMBER
PPM00019185

5f. WORK UNIT NUMBER
EF123149

7. PERFORMING ORGANIZATION NAME(S) AND ADDRESS(ES)
University of Illinois at Urbana-Champaign
1110 W. Green Street
Urbana, IL 61801-3620

8. PERFORMING ORGANIZATION REPORT NUMBER

9. SPONSORING / MONITORING AGENCY NAME(S) AND ADDRESS(ES)
Air Force Research Laboratory
Space Vehicles Directorate
3550 Aberdeen Ave SE
Kirtland AFB, NM 87117-5776

10. SPONSOR/MONITOR'S ACRONYM(S)
AFRL/RVSV

11. SPONSOR/MONITOR'S REPORT NUMBER(S)
AFRL-RV-PS-TR-2017-0169

12. DISTRIBUTION / AVAILABILITY STATEMENT
Approved for public release; distribution is unlimited.

13. SUPPLEMENTARY NOTES

14. ABSTRACT

We assembled nanocapacitors with large dielectric strength to a nanoscale rechargeable battery. We fabricated arrays of one-, two- and three-dimensional synthetic atoms and comparison of its performance data with theoretical predictions. We investigated recovery of alumina nanocapacitors after high-voltage breakdown. Previously we had discovered that Al_2O_3 nanocapacitors can self-repair. Recently we discovered that our newly fabricated SiO_2 nanocapacitors can self-repair. We found a significant reduction of leak currents and an increased dielectric strength due to coulomb blockade in nanocapacitors. On the theory side, we are making great progress. We computed the leak currents for synthetic atoms in one, and three dimensions. We filed several disclosures.

15. SUBJECT TERMS
ultracapacitors, high specific energy, space power, specific power > 50 Wh/kg or 50 Whr/kg

16. SECURITY CLASSIFICATION OF:			17. LIMITATION OF ABSTRACT	18. NUMBER OF PAGES	19a. NAME OF RESPONSIBLE PERSON
a. REPORT	b. ABSTRACT	c. THIS PAGE			Jessica Buckner
Unclassified	Unclassified	Unclassified	Unlimited	44	19b. TELEPHONE NUMBER *(include area code)*

--- This Page Intentionally Left Blank ---

TABLE OF CONTENTS

LIST OF FIGURES

ACKNOWLEDGMENTS

This material is based on research sponsored by Air Force Research Laboratory under agreement number FA9453-14-1-0247. The U.S. Government is authorized to reproduce and distribute reprints for Governmental purposes notwithstanding any copyright notation thereon.

DISCLAIMER

(This page intentionally left blank)

1. SUMMARY

The energy density in chemical bonds is a theoretical limit for most energy storage systems. For example, in fly wheels the energy density of the bonds limits the tensile strength of the material and therefore limits the energy storage capacity. In compressed air systems, the energy density of the bonds in the wall material limits the compressive strength and therefore limits the energy density of the system. The proposed technology takes advantage of quantization phenomena to design nanocapacitor storage devices which reach that limit and go beyond.

In Task I (9 months), we assembled nanocapacitors with large dielectric strength to a nanoscale rechargeable battery. The following parameters were investigated experimentally: maximum energy density, leak currents.

In Task II (9 months) we fabricated one-, two- and three-dimensional synthetic atoms and compared their performance data with theoretical predictions. We studied recovery after failure and likelihood of cascading failures. Simultaneously, nanocapacitors with a particularly large dielectric strength were fabricated with radio frequency (RF) sputtering in our laboratories. The reduction of leak currents and increased dielectric strength due to Coulomb blockade was studied theoretically on 1-dimensional synthetic atoms (cathode-anode-cathode nanocapacitors).

In Task III (9 months), we investigated recovery of alumina nanocapacitors after high-voltage breakdown. Previously we had discovered that Al_2O_3 nanocapacitors can self-repair. Recently we discovered that our newly fabricated SiO_2 nanocapacitors can self-repair too. Nanocapacitors with a particularly large dielectric strength will be assembled into an energy storage device and tested. The data from task I were used to improve the performance of the energy storage device. A lab prototype of an optimized energy storage device with an assembly of nanocapacitors will be completed for external testing. First lab prototypes of energy storage made of synthetic atoms and of stacks of nanocapacitors will be assembled and tested.

In Task 4 (9 months) Multi-dimensional synthetic atoms was studied theoretically.

2. INTRODUCTION

We are conducting research into the energy storage in nanocapacitor arrays. Nanocapacitors are expected to be fully functional in a large temperature range, starting from space temperatures in the shadow of the Earth to the melting temperature of tungsten (3422 ºC). In contrast to batteries with electrolytes, nanocapacitor batteries can be fully charged and discharged billions of times without any loss of efficiency. Nanocapacitor batteries can be fully integrated with advanced electronics. However, there are several hurdles to overcome, before nanocapacitor batteries can replace Li-ion batteries and super-capacitors:

(1) The maximum energy density is currently much less than in Faradic systems.
(2) Tunneling currents, field emission currents, and other leak currents reduce the efficiency of nanocapacitor batteries.
(3) The power density is much larger than in Faradic systems and this is a potential safety problem.

We investigate several hypotheses to overcome these hurdles:

(1) The dielectric strength and the maximum energy density depend on the gap size. The dielectric strength of capacitors with gap sizes in the nm range is increased by 3 orders of magnitude. The energy density is limited by the tensile strength of the electrodes. Consequently, an array of a large number of nanocapacitors has a much larger energy density than a single, large capacitor with the same weight and volume.
(2) In 3-layer, cathode-anode-cathode nanocapacitors (synthetic atoms) leak currents can be suppressed with Coulomb blockade. When Coulomb blockade occurs, quantum pressure keeps the electrons away from the anode, like the electron is kept away from the nucleus in a hydrogen atom.
(3) Dielectric nanocapacitors can recover after breakdown. If the recovery is fast, cascading failures can be suppressed.

We are studying:

(1) The efficiency of energy storage in nanocapacitors arrays as a function of temperature, the number of charge/discharge cycles, and the average energy density;
(2) Leak currents in arrays of synthetic atoms and evidence for Coulomb blockade;
(3) The recovery time after breakdown and the probability of cascading failure in nanocapacitor batteries.

The long-term goal of this work is to create a new battery type which exceeds the energy density, efficiency, reliability and safety standards of chemical batteries and is fully operational at a large temperature range.

3. TASK I: ASSEMBLE NANO-CAPACITORS WITH LARGE DIELECTRIC STRENGTH TO A RECHARGEABLE BATTERY

3.1. Methods, Assumptions, and Procedures

We used two different fabrication methods. In one fabrication method the substrate was silicon. In the other fabrication method the substrate was glass.

3.1.1 Fabrication method 1

We bought silicon wafers from Silicon Quest (see Figure 1). The bare silicon wafers with the natural passivation oxide layer are oxidized with a furnace (see Figure 2) to various thicknesses.

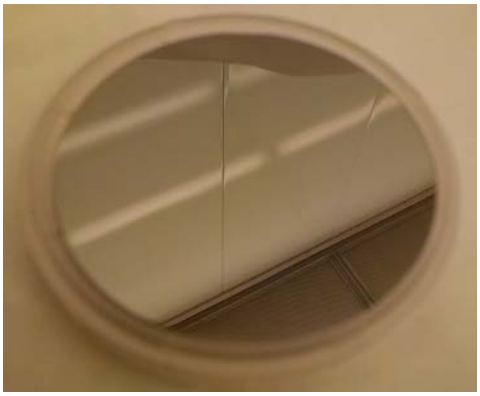

Figure 1. Bare silicon wafers with a natural passivation oxide layer.

Figure 2. Photo of our oxidation furnace.

Then we checked the thickness of the oxide layer with ellipsometry (see Figure 3). Finally, we use a shadow mask in the electron beam evaporator (see Figure 4) to deposit circular metal islands on the oxide. Figure 5 shows an image of a nanocapacitor, after using the electron beam evaporator to deposit chromium and gold.

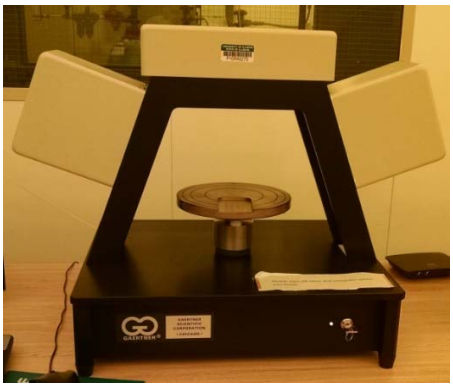

Figure 3. This ellipsometer measures the thickness of the oxide layer.

Figure 4. This electron beam evaporator deposits various metals.

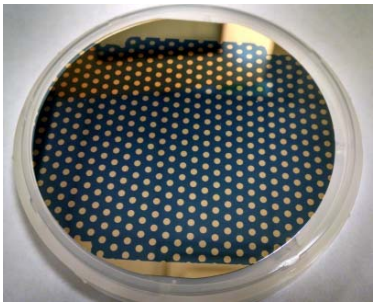

Figure 5. A silicon dioxide layer with gold island.

The Scanning Electron Microscope (SEM) in Figure 6 is used to determine the quality of the islands (see Figure 7).

Figure 6. Hitachi S4700 scanning electron microscope

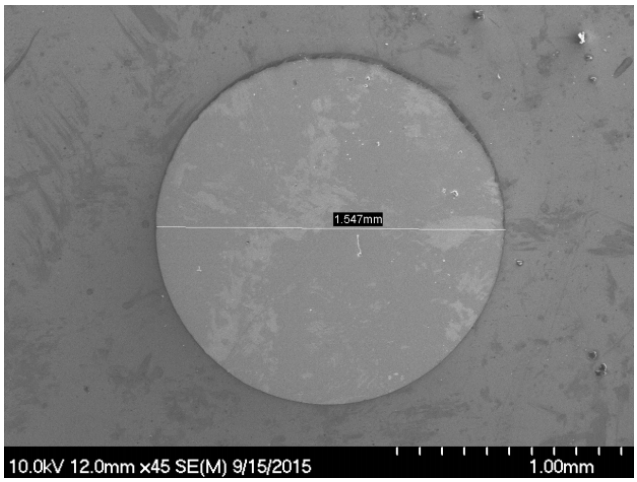

Figure 7. SEM image a nanocapacitor (top view of gold islands with diameter 1.547mm).

We find that in the new samples the dielectric strength is more reproducible and larger. Further we find that dielectric strength is larger for thinner oxide layers (see Figure 8). The dielectric strength determines the maximum energy density.

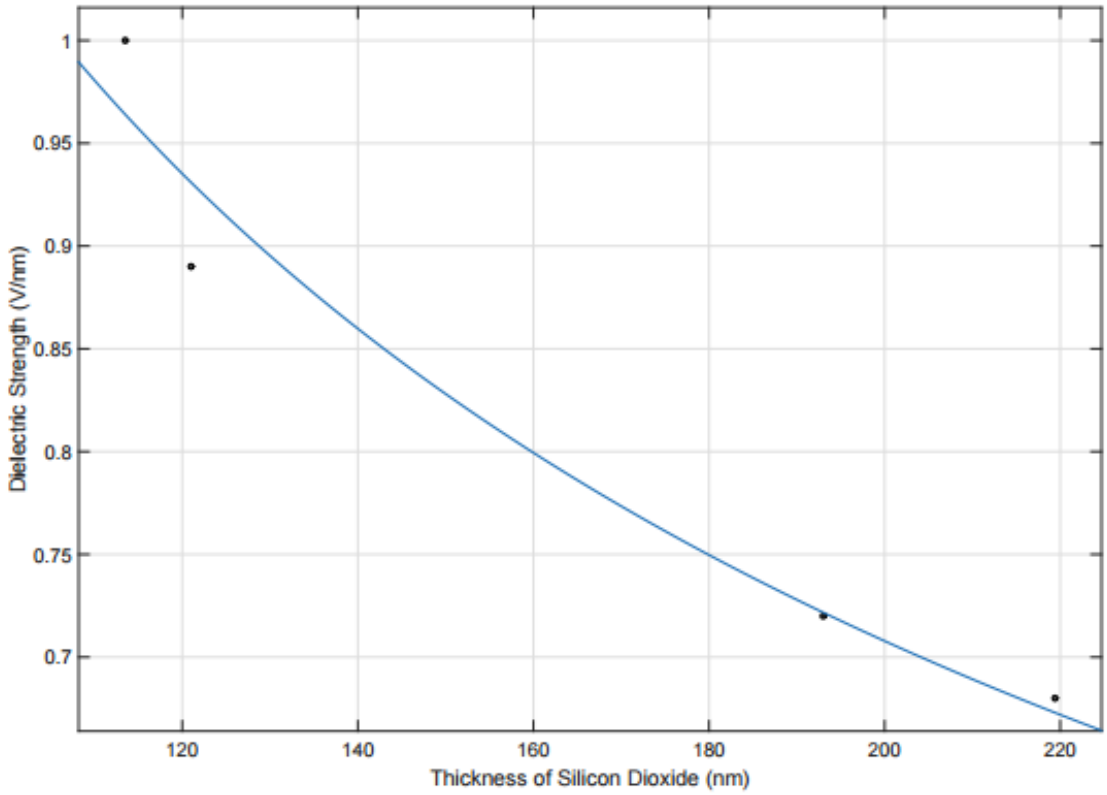

Figure 8. Plot of average dielectric strength verses thickness of silicon dioxide nanocapacitors.

3.1.2 Fabrication method 2

We fabricated a multi-layer nano-capacitor energy storage systems and tested them. Figure 9 is a sketch of the system on a glass substrate. The side view on the left and the top view is on the right.

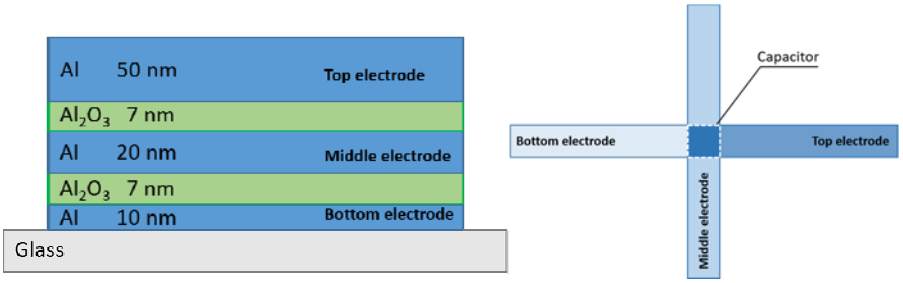

Figure 9. Sketch of 3-layer nano-capacitor system.

Figure 10 shows photos of the as fabricated device.

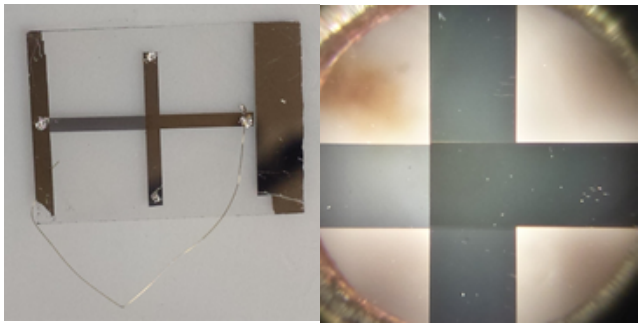

Figure 10. Photos of the 3-layer nano-capacitor system described in Figure 1.

Al deposition is done by with e-beam evaporation. Al_2O_3 deposition is done in Atomic Layer Depostion (ALD) system. Metal shadow masks are used to make the pattern. The capacitance was measured at room temperature. The amplitude of the test signal was 0.5 V. The frequency was 120 Hz:

Bottom-Middle electrode capacitance: $C_{B\text{-}M}$*= 4.62 nF*

Middle-Top electrode capacitance: $C_{M\text{-}T}$*= 4.18 nF*

Total capacitance (top-bottom electrodes are connected with gold wire): $C_{BT\text{-}M}$*= 8.80 nF*

The measurements confirmed that $C_{BT\text{-}M} = C_{B\text{-}M} + C_{M\text{-}T}$. The measured results are consistent with the theoretical estimates if $\approx\varepsilon 4$. This is close to the theoretical value, ε=4.5.

3.2 Results and Discussion

We found that a stack of nanocapacitors has anticipated energy storage capacity and extremely small leak currents. This might be due to Coulomb blockade. Preliminary results predict a reduction of 4 orders of magnitude. The blue line is a graph which includes the scaling of the field enhancement factor with the thickness of the dielectric. [1]

3.3 Conclusion

We conclude that there are no apparent obstacles in fabricating a micro-battery with many layers.

4. TASK II: FABRICATE ARRAYS OF ONE-, TWO- AND THREE-DIMENSIONAL SYNTHETIC ATOMS AND COMPARISON OF ITS PERFORMANCE DATA WITH THEORETICAL PREDICTIONS.

4.1. Methods, Assumptions, and Procedures

One of the most prominent features of synthetic atoms is charge storage in the space between the electrodes [1, 2]. Hysteresis in the I-V curve (current versus voltage plot) is a footprint of charge storage in the dielectric, because charge originating from the dielectric has a larger time scale. The I-V curve for the multi-layer capacitor shown in Figure 11 has hysteresis. This supports the hypothesis that the theory of synthetic atoms is a good model for such multilayer nano-capacitors.

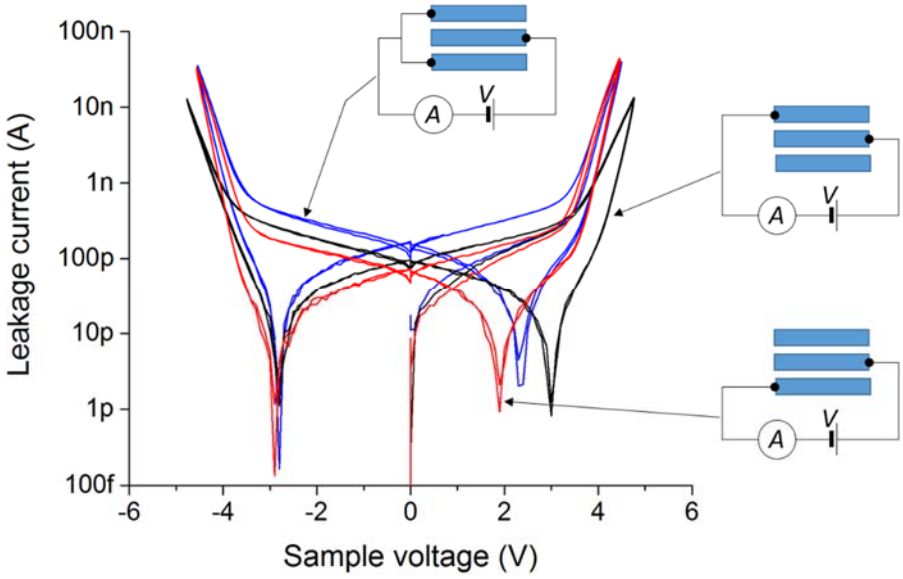

Figure 11. I-V curves of the 3-layer nano-capacitor system.

4.1.1. Charge Storage between the electrodes

Figure 11 shows the I-V curves of a 3-layer nano-capacitor system. The black and red curves are the I-V curves of the two 2-layer capacitors. The blue curve is the I-V curve of the 3-layer system. The leak current of the 3-layer system is not additive for negative voltages and particularly small. These data seem to verify the prediction that synthetic atom store charge in the dielectric.

For practical applications, it is conventionally assumed that most of the electric charge in a standard metal/insulator capacitor is typically stored on the metal plates. However, in a fully

charged capacitor there is usually some extra charge absorbed by the dielectric media, associated with either the displacement of charges, or from movement of electrons from the metallic plates of the capacitor into the dielectric layer separating the plates. Such charge penetration into the dielectric is driven by the strong electric field occurring in the dielectric spacer of a nanocapacitor. This absorption of electric charge by dielectric is a well-known and well-studied phenomenon [3-5]. Generally, there are several competing mechanisms by which the charge can be retained. Two of these mechanisms: hindered dipole rotation and displacement of ions in dielectric, do not involve any transfer of charge between the metal plates and the dielectric [4, 5]. Additionally, there is always the possibility of charge penetration into the dielectric due to the movement of hopping charges, i.e. the tunneling of electrons between the metal plates and some localized charge traps in the dielectric [6-8].

Due to dielectric absorption, the discharging of a capacitor is essentially a multiple-stage process, with charge deposited on metal and charge acquired by dielectric, occurring on different time scales. Obviously, the time scale for the discharge of the plates is controlled by the value of the shunting resistor, *R*. Typically the loss of charge accumulated on metal plates is a very fast process, described by the exponential law with characteristic time completely determined by the capacitance and the total resistance of the short circuit. In contrast, the removal of charge accumulated by dielectric is a considerably slower process, generally described by relaxation theory [9].

4.1.2. Sample fabrication and measurements

An aluminum film is deposited on a glass substrate and covered with alumina (Al_2O_3), which serves as the dielectric layer of the capacitor. The top electrode is a single layer of graphene. Graphene has metallic conductivity and acts here as a metallic plate of the capacitor. Thus, effectively, the sample consists of two identical capacitors, of the type Al-Al_2O_3-graphene, connected in series. Thus, the obtained capacitance is twice smaller than the value computed for just one such capacitor. Note that the source of voltage used here is adjustable, i.e., it can be controlled from the computer and can be set to zero or to any desired value.

The nanocapacitors used in this study were made with a d=50 nm thick Al film coated by a 7 nm layer of Al_2O_3 and a single layer of graphene. The sample schematic is shown in Figure12. A picture of the device is shown in Figure 13. The length of the strip was L=10 mm and the width is w=1 mm. Thus, the expected capacitance was $C=\varepsilon\varepsilon_0 Lw/d=12.6$ nF. The actual measured value was 10 nF, which is close.

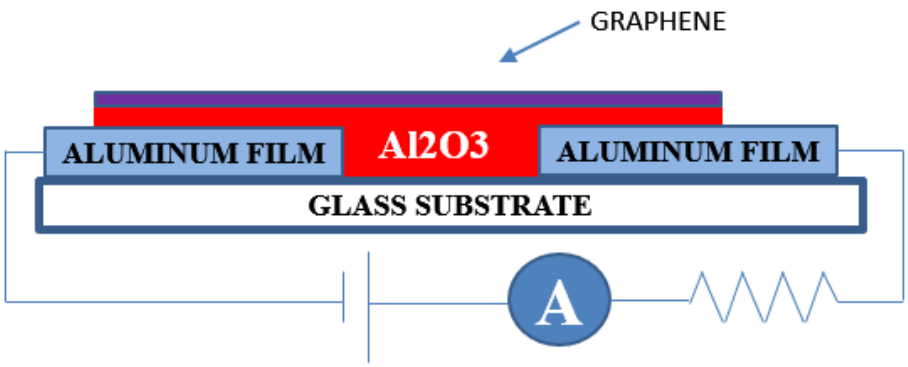

Figure 12. Schematic of a graphene nano-capacitor.

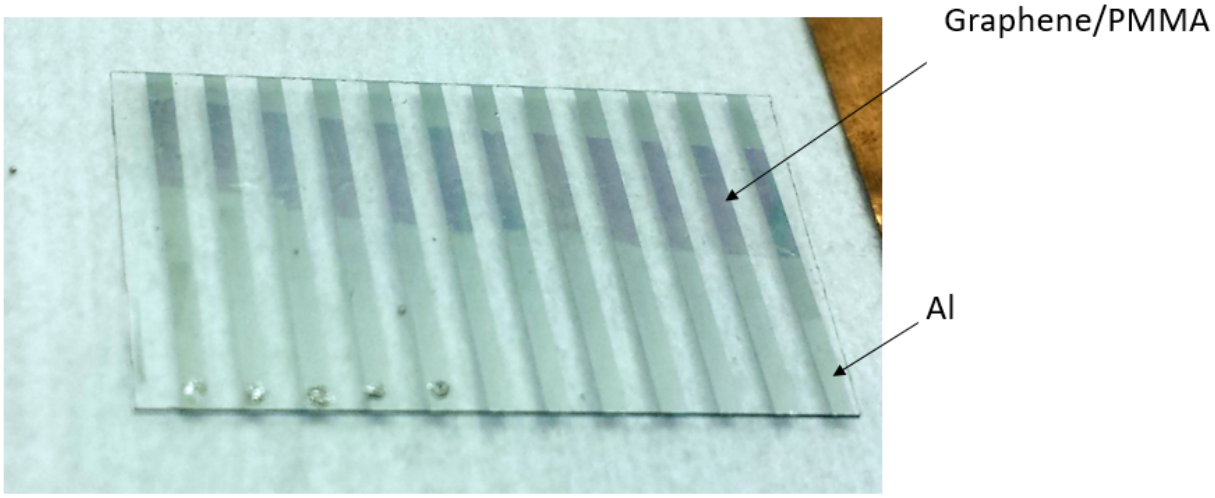

Figure 13. A picture of the device described in Figure 12.

To measure the charge Q, stored on the capacitor, we apply voltage V, of the order of a few volts, and wait a few minutes. Then the voltage on the battery is changed to zero and the current is measured as a function of time. Note that in equilibrium the current is zero since the capacitor does not provide a path for a dc current. Thus, the current we detect is a transient phenomenon, occurring either after the voltage is set to a constant nonzero value or after the voltage is set to zero. It is interesting to note that in a wide range of voltage the current approaches zero with time even if the voltage is above zero. This provides strong evidence that our capacitors are not leaky, i.e. the leakage current through the dielectric is zero.

4.2. Results and discussion

Figure 14 shows I-V curves for such devices.

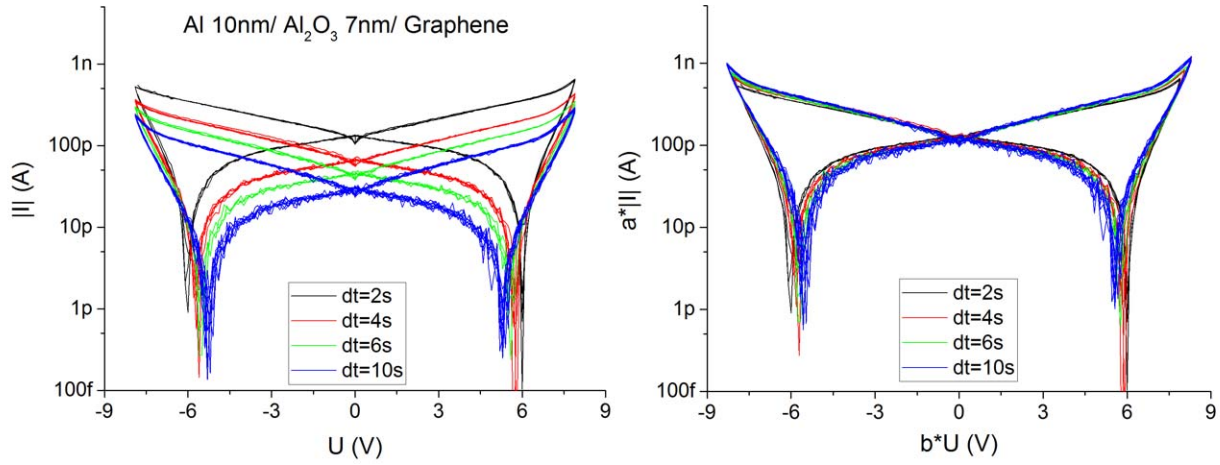

Figure 14. I-V curve (left) and rescaled I-V curve (right) of a graphene nano-capacitor.

The capacitor discharge current is shown in Figure 15.

The initial regime is the exponential discharge. In this case the current decays exponentially with time. But at about 9 s on the time axis a new regime begins, which is a power-law decay of the current. It is clear in the log-log plot shown in Figure 15, where the second regime appears to be a straight line.

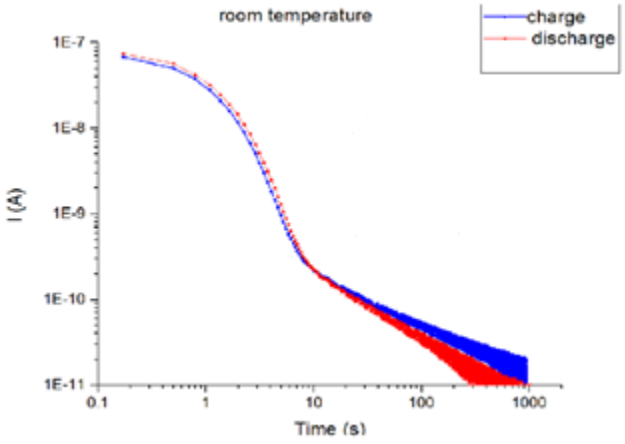

Figure 15. The discharge current measured in the circuit shown in Figure 12.

A more detailed study of the discharge process is shown in Figure 16. The discharge current is shown for three different voltages. In all three cases the dependence is proportional to $I(t)\sim 1/t$. The exact power of this power law decay can be either slightly smaller or slightly larger than the generic value of -1.In this case the series resistor was lower so that the current drop occurred faster. So, when the measurement was started only the power low residual discharge (stage 2) is observed. It shows a power-law dependence quite clearly.

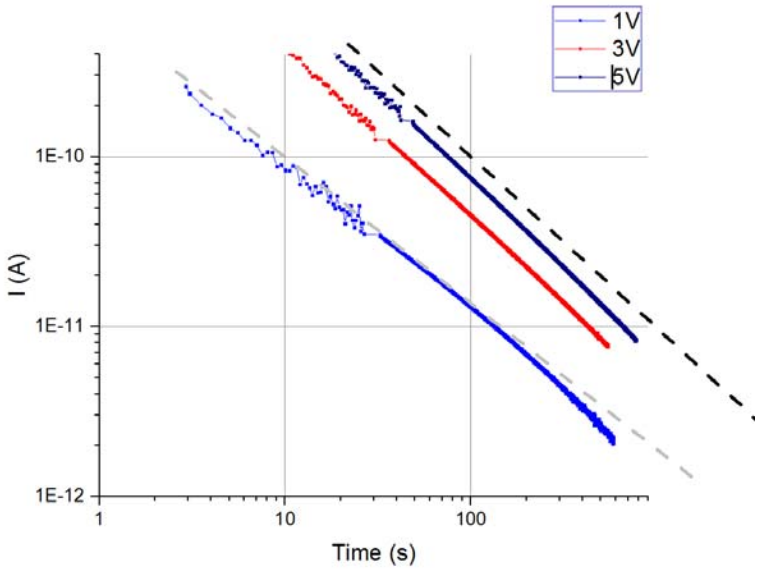

Figure 16. The graphene nanocapacitor discharge current versus time.

It is interesting that the integration of the current, which gives the charge stored in the dielectric, $Q = \int_0^\infty I(t)dt$ gives very large values, which are near the value of the charge stored on the capacitor plates, $Q_p=VC$. We attribute this fact to the small thickness of the dielectric, which is of the order of a few nanometers. We speculate that at the high electric field created in the reported experiments, of the order of *0.1-1 V/nm*, the electron can enter the dielectric by quantum tunneling. Thus, the charge penetration is very massive. For comparison we note that in regular capacitors the charge stored in the dielectric is only a few percent of the Q_p charge.

4.2.1. Bulk charge measurements

The most interesting result of this work is the observation of a large charge stored in the volume of the dielectric medium of the capacitor. We find that the charge stored in the dielectric, Q_d, is approximately equal to the charge, Q_p, stored on the plates of the capacitor. The capacitor plate charge Q_p is defined by the geometric properties of the plates as well as the dielectric constant of the dielectric, namely $Q_p=VC$, where the geometric capacitance is $C=A\varepsilon\varepsilon_0/d$. It is possible to measure these two charges, Q_p and Q_d, separately since the discharge of the capacitor is controlled

by the resistor R shunting the capacitor while the dielectric volume charge Q_d decreases at a much slower rate, which is defined by some internal process of the charge migration in the dielectric.

To define the charge Q_d we measure the current and then integrate it. The total charge is defined as $Q = Q_p + Q_d = \int_0^\infty I(t)dt = \int_0^\infty I_d dt + \int_0^\infty I_p dt$. The current I(t) represent the total current flowing from the capacitor. Technically speaking we cannot measure I_d and I_p separately. Yet it is clear that the current I_p can drop quickly, namely at a timescale tau, which we can control by choosing the series resistor R. After the plates are discharged almost completely we can assume that $I \approx I_d$ and define the dielectric charge approximately as $Q_d = \int_0^\infty I_d dt$. Note that this is a lower bound on the dielectric charge. Yet, as we see below, even this low-bound estimate gives a dielectric charge which is approximately equal to the volume charge.

In other words, it is due to a discharge of both Q_p and Q_d. Therefore, to measure the dielectric charge we start the integration at the time when the plate charge is greatly reduced. The time scale of the discharge of the capacitor is $\tau = RC$. In other words, $Q_p = CV_0 \exp[-t/\tau]$, where V_0 is the initial voltage. The corresponding current, as a function of time t is $I_p = (CV_0/\tau)\exp[-t/\tau] = (V_0/R)\exp[-t/\tau]$.

4.2.2. Discussion

Fundamentally, the time-dependent response of a system to a step-function removal of constant stress is most conveniently defined through the Fourier transform of the frequency-dependent response, which is known for a large variety of mechanisms of dielectric absorption. As suggested by Jonscher [9], one can generally distinguish between two fundamentally different types of dielectric response. The first type, termed 'dipolar', is a generalization of the Debye concept of polarization due to the hindered movement of ideal dipoles. This type of polarization leads to zero residual polarization after discharge, with the time dependence of the charge described by the exponential law ~ $exp(-\omega_p t)$, where ω_p is the loss peak frequency of the dielectric response in the frequency domain. The second type of response describes the behavior of a system where polarization is dominated by slow movement of hopping charge carriers, which is relevant for the charge accumulation due to tunneling of electrons to localized states in dielectric. This type of dielectric response has a fractional power law time dependence ~ $t^{-\alpha}$, and is characterized by finite residual polarization of the system.

In practical applications, the measured property is usually not the residual polarization or the residual charge, but the discharge current. Generally, for times much longer than the RC relaxation time of the capacitor, the discharge current due to different mechanisms of charge retention by dielectric can be described by the fractional power law ~ $t^{-\alpha-1}$, with different mechanisms resulting in different values of the power α [6]. The varying time dependence of the discharge currents resulting from different mechanisms of charge absorption can in principle be used to eliminate some mechanisms for a particular dielectric, or to analyze the relative contributions of those mechanisms. Additionally, beside the different time dependences, some mechanisms are characterized by dissimilarity between the charging and discharging processes, which can be further used for the same purpose. Specifically, the trapped volume charge formed through charge

injection, possibly by tunneling [10], is absorbed and released on different time scales, making its contribution apparent if a large hysteresis is observed between the charge and discharge currents.

In practical terms, the observed discharge current can be formally split into a contribution from resistance-capacitance (R-C) relaxation and the residual current due to dielectric relaxation or the charge stored in the dielectric:

$I(t) = I_o [\, e^{-(t/RC)} \,] + i(t)$. The residual current can be further defined as $i(t) = At^{-\alpha}$.
Experimentally we find that $\alpha \sim 1.s$

4.2.3. Model 1: Charge storage in dielectric traps

We propose a model which can reproduce the essential feature seen in most experiments. Namely the model can predict the power law dependence $I(t) \sim t^{\alpha}$, with $\alpha \approx 1$.

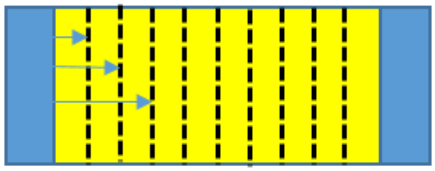

Figure 17. Sketch of the dielectric trap model.

The model is illustrated in Figure 17. A plane capacitor is formed between two metallic plates (blue) and a dielectric spacer (yellow). The position of the charge traps is shown by dashed lines. For the simplicity of the argument we assume that the charge traps are positioned along the dashed lines, and with the position along the horizontal axis $x_n = dn$, where $n = 1,2,3,...$ is an integer, and d is the distance between neighbor planes where the defects are concentrated. Let us assume that the left metallic plate is negatively biased, and the electrons propagate to the right, by means of quantum tunneling [10] (see the horizontal blue arrows). The tunneling probability to the first plane (top arrow) with localized charge traps is $p1 = Cexp[-kx1] = Cexp[-kd]$, the tunneling rate to the second plane (second arrow) is $p2 = Cexp[-kx2] = Cexp[-2kd]$, and the tunneling rate to the third plane (bottom arrow) is $p3 = Cexp[-kx3] = Cexp[-3kd]$, etc. Note that the number of planes is much larger than what we show on the schematic of Figure 17. The number of planes can be estimated as the thickness of the dielectric, *7 nm*, divided by the distance between the atoms, *0.3 nm*. Such rough estimate gives about *200 planes* with charge traps.

Let us assume now that a voltage is applied, and the charge begin to tunnel into the dielectric. Assume that we wait time t and then estimate how many planes are charged. Let us estimate the number of charge trap planes which can be charged within time t. It can be said that the time needed to fill out a plane n of charge traps is $Tn = M/pn$, where M is the total number of charge traps in a plane (assumed to be the same number for all planes). So, a plane of charge traps will be filled within time t if $t > Tn$. The largest number of the plane which will be filled within time t is $Tn = t$ *or* $pn = M/t$ or $Cexp[-kxn] = M/t$. Thus the volume charge will spread up to the charge trap plane with the position $xn = -(1/k)ln[M/Ct]$ or $xn = (1/k)ln[t(C/M)] = (1/k)ln[t] + C2$.

The total charge will be $Q(t)=Mn=Mxn/d=(M/kd)ln(t)+C3$. Finally, the current is $I(t)=(M/kD)t^{-1}$, as is observed in experiments.

4.2.4. Model 2: Charge storage in eigenstates of the quantum well created by the dielectric

There are two primary mechanisms by which charge flows in a quantum well under an electric field: Fowler-Nordheim emission (also called cold field emission or CFE) and spontaneous emission. Here, we consider the dynamics of the CFE current of a discharging nanocapacitor.

The cold field emission current is:

$$J = -\frac{\alpha_1 \nu}{\phi} (\gamma F)^2 \exp\left(\frac{\alpha_2 \phi^{3/2}}{\gamma F}\right) \tag{1}$$

Where F is the macroscopic field strength, Φ is the work function of the metal. γ is the dimensionless field enhancement factor, where is $\gamma \approx 1$ for w < 30 nm. $\nu \approx 1$ the dimensionless correction coefficients determined from a numerical analysis of the surface of the metal (or a more careful analytical treatment). α_1 and α_2 are the Fowler-Nordheim constants.

Consider a two-plate capacitor separated by a width of w and with a potential difference of ΔV. The field strength between the plates is $F = \Delta V/w$ and the charge density on the plates is $\sigma = \varepsilon F$. If the capacitor is disconnected from the potential difference, current J will flow which will drive a change in the field strength. Thus, the previous equations can be rewritten as a differential equation for the field strength noting that for two parallel plates: $J(t) = \varepsilon F'(t)$

$$F'(t) = -\frac{\alpha_1 \nu}{\epsilon \phi} (\gamma F(t))^2 \exp\left(\frac{\alpha_2 \phi^{3/2}}{\gamma F(t)}\right) \tag{2}$$

This Ordinary Differential Equation (ODE) can be solved analytically with the initial condition $F(0) = F_0$ and solutions take the form:

$$F(t) = \left(\frac{\alpha_2 \phi^{3/2}}{\gamma}\right) \log\left[\exp\left(\frac{\alpha_2 \phi^{3/2}}{\gamma F_0}\right) + \frac{\alpha_1 \alpha_2 \gamma \nu \phi^{1/2}}{\epsilon} t\right]^{-1} \tag{3}$$

We find:

$$J \approx -\frac{\alpha_2 \epsilon \phi^{3/2}}{\gamma t} \log\left[\frac{\alpha_1 \alpha_2 \gamma \nu \phi^{1/2}}{\epsilon} t\right]^{-2} \tag{4}$$

This expression for the current (roughly) exhibits the $J \sim 1/t$ behavior as previously measured. In the other case, where:

$$\exp\left(\frac{\alpha_2\,\phi^{3/2}}{\gamma\,F_0}\right) >> \frac{\alpha_1\,\alpha_2\,\gamma\,\nu\,\phi^{1/2}}{\epsilon}\,t \tag{5}$$

The current is approximately constant:

$$J(t) \approx -\frac{\alpha_1\,\gamma^2\,F_0^2\,\nu}{\phi}\,\exp\left(\frac{\alpha_2\,\phi^{3/2}}{\gamma\,F_0}\right) \tag{6}$$

Figure 18 shows a typical dynamics of the cold field emission current versus time for an initial field strength of $F_0 = 1$ *eV/nm*.

Thus, there is a "critical" time, τc, when the current transitions from being relatively constant to falling off like $1/t$:

$$\tau_c = \frac{\epsilon}{\alpha_1\,\alpha_2\,\gamma\,\nu\,\phi^{1/2}}\,\exp\left(\frac{\alpha_2\,\phi^{3/2}}{\gamma\,F_0}\right) \tag{7}$$

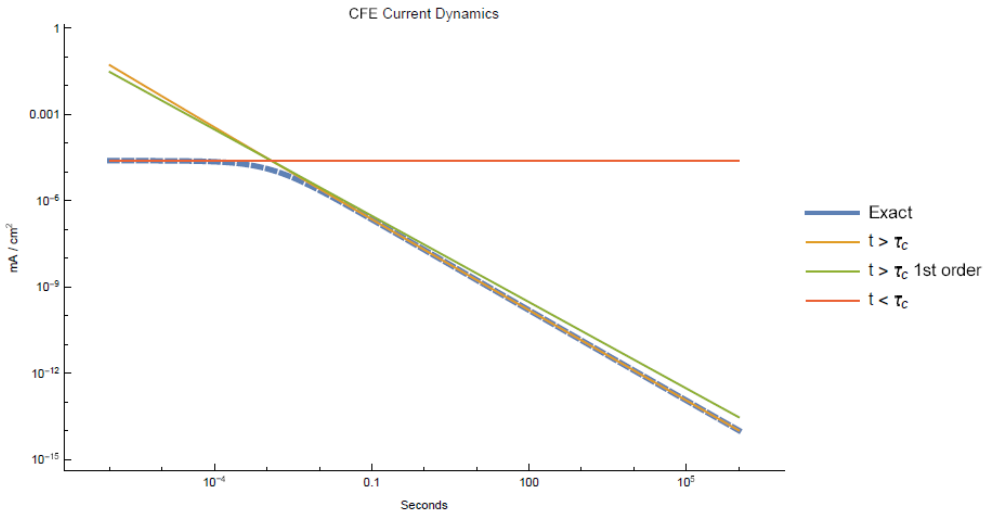

Figure 18. The CFE current as a function of time and the approximation functions.

Figure 19 shows the break down time versus the field enhancement facto for typical parameter values.

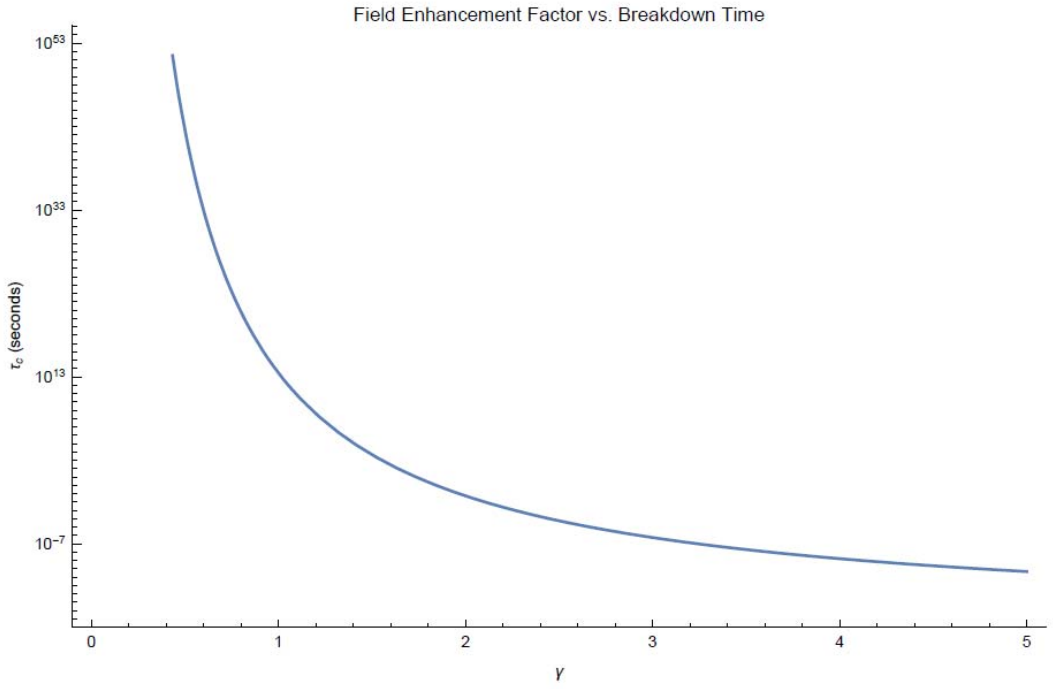

Figure 19. The breakdown time, τ_c versus field enhancement factor γ.

4.2.5. Estimation of the leakage current

Based on the model presented above, and the fact that the power law behavior of the current was observed at all time scales tested, one should assume that the electrons cannot tunnel, within the time scale of the experiments, through the entire thickness of the dielectric. Thus, the leak current should be very small. In order to determine the leakage current experimentally we have charged our capacitors up to *3 V*, then disconnected the capacitor from the charging circuit and allowed it to sit without being connected to anything for time Δt. In this time interval the discharge of the capacitor was happening only through the leakage current in the dielectric. The results are shown in Figure 20. The discharge is done not immediately after the capacitor was charged but after some delay t_2. The delay for the plotted curves, from the top to the bottom, was t_2*=2 min, 10 min, 1.5 h, 4h, 23 h.* The exponential discharge fit is done for the case of t_2*=4h*. The initial current was *22.3 nA,* according to the fit.

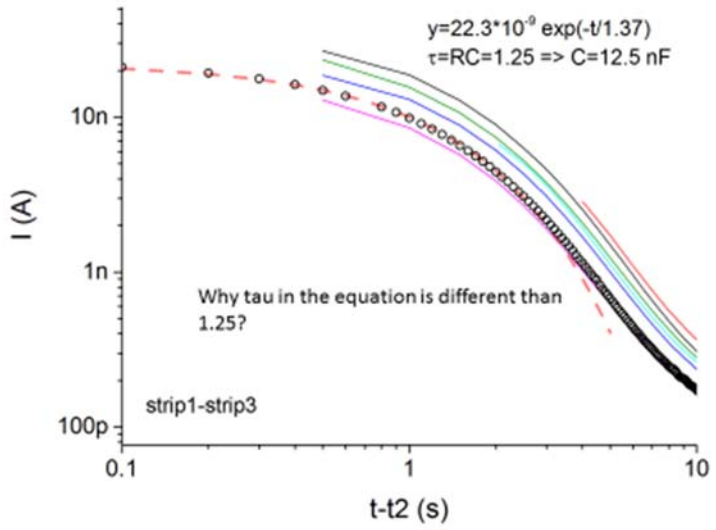

Figure 20. The discharge current of a capacitor through a resistor of R_s=100 MOhm.

The initial charge was $Q_1=CV_1$. The initial voltage is $V_1=I_1*Rs$, where the shunting resistor is $Rs=100$ *MOhm*. The initial current is *22.3 nA*. so, the initial voltage is $V_1=2.23$ *V*. Thus within 4 hours the charge dropped by $\Delta Q=C(V_0-V_1)$ =*8.4 nC*. So, the leak current roughly estimated is $I\_leak=\Delta Q/\Delta t=0.6$ *pA*. With this level of leakage, the discharge time is a few hours. Further improvements of the dielectric will be needed to store charge over longer time intervals. In the future we plan to test the effect of low temperatures. It is expected that leakages will be reduced at low temperatures.

4.2.6. Total charge stored in the dielectric

Here we present an example of our data analysis intended to define the amount of charge stored on the dielectric. The charge on metal (total charge from the exponential current) is well defined, simply because it can be fitted with an exponential function and then extrapolated to zero time and to the infinity. Such extrapolated exponent can then be easily integrated mathematically since the integral of the exponent is finite. On the other hand, there is much noise in the measured current data so that the overall charge is less precisely defined. Although the noise is integrated out to zero, since it is Gaussian and the fluctuations occur to the positive direction with the same probability as the negative direction. On the other hand, there is another inaccuracy, related to the fact that the measurement apparatus (Keithley 6517) gives some offset. To eliminate the offset contribution we determine the current at very large times. Then we subtract this offset current from the raw data, only after that the integration is done. Thus, the obtained estimate to the stored charge is $Qd=3.0\ 10^{-8}$ *C=30 nC.* On the other hand, the charge stored on the metallic plates of the capacitor is $Q_p = CV$. The applied voltage was $V=3V$. The capacitance was estimated from the discharge curves and was found *C=12.5 nF*. So the charge on the plates is $Q_p=37.5$ *nC*. We find that *Qd* is just slightly lower than Q_p. Thus, the results indicate that the dielectric can double the efficiency of the energy storage in nano-capacitors. The total stored charge is *67.5 nC* according to our analysis. Thus, the

total energy is $E=Q_pV/2=100\ nJ$. The energy density is $E/A/d1=48\ MJ/m^3$. This can be converted to the energy per unit mass. The density of Al_2O_3 is 3.95 g/cm^3, so the density is 3950 kg/m^3. Thus, the mass of the dielectric is *8.4 nano-gramm*. So, the energy density is *12 MJ/kg*. This is about four times less than for gasoline. Still, this result, taken together with the observed slow discharge, suggests that nano-capacitors can be used for energy storage.

4.2.7. Three-dimensional synthetic atoms: The point of closest distance of two perpendicular plates which almost touch

Two perpendicular gold foils are attached to a commercially available nano-positioning device. The device pushes the foils towards each other. When an electrical contact is established, the motion is reversed, to establish a gap of a desired size. A typical gap is of the order of ~100 nm, so it is not visible on the photograph.

We measured break down voltage as a function of the distance between gold plates (see Figure 21 and Figure 22). The edges were electropolished after mechanical polishing before measurements. Applied voltage was removed immediately after breakdown. The approach of edges was stopped as soon as they touched each other. Then the plates were pushed to the desired distance.

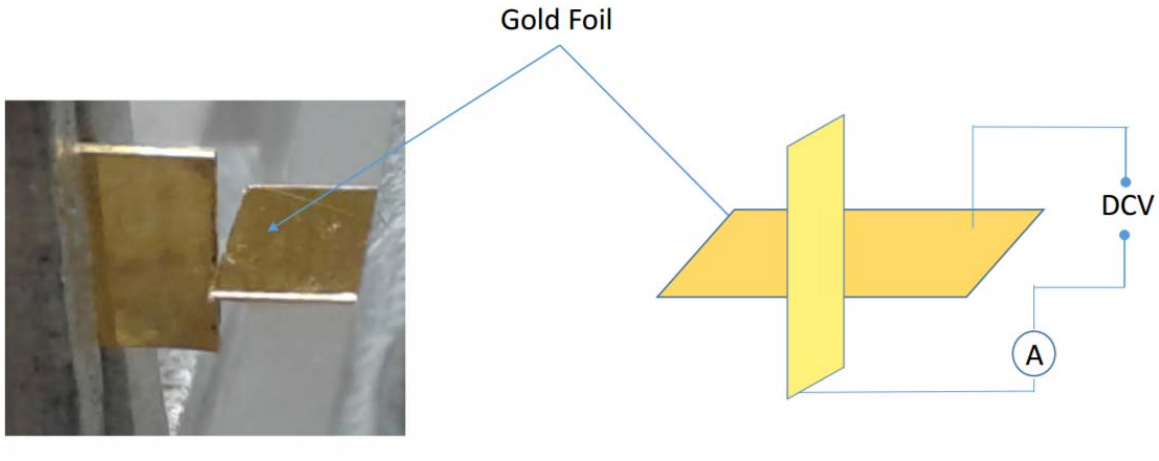

Figure 21. Schematics of a 3D synthetic atom: Two perpendicular gold foils.

The experiments (see Figure 22) suggest that vacuum capacitors can reach an average electric field of 2.5 GV/m, which is a factor of 5 larger than dielectric capacitors. We assume that the dielectric material has a larger tensile strength.

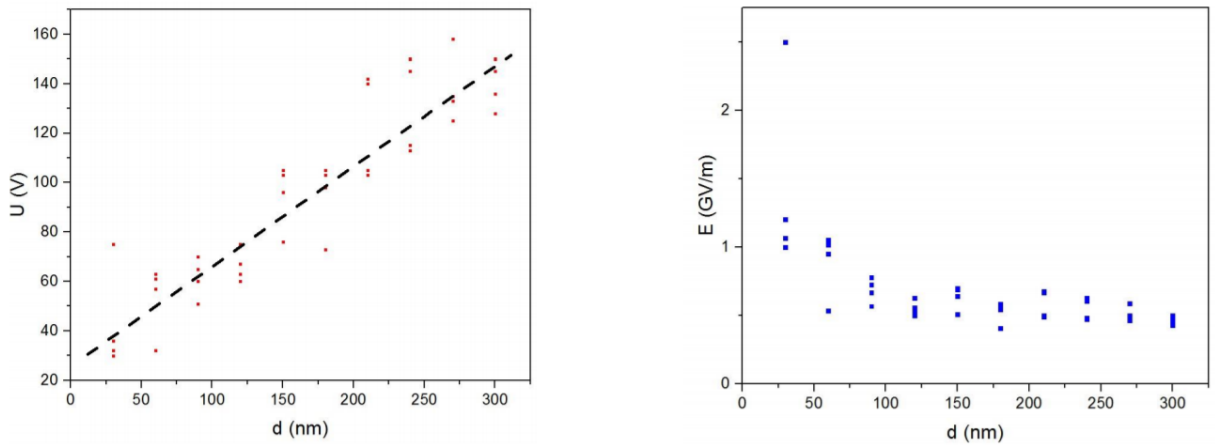

Figure 22. The breakdown voltage (left) and the corresponding dielectric strength versus the distance (right).

4.2.8 Two-dimensional synthetic atoms: A Spindt ridge

Next we designed a two-dimensional synthetic atom with a linear cathode and a planar cathode (see Figure 23-25). The anode is a Spindt ridge in a trench in a SiO_2 layer and the counter electrode is a planar graphene electrode (Wire width ~130 nm Spindt tip height ~200 nm Distance from the tip to the graphene ~100 nm).

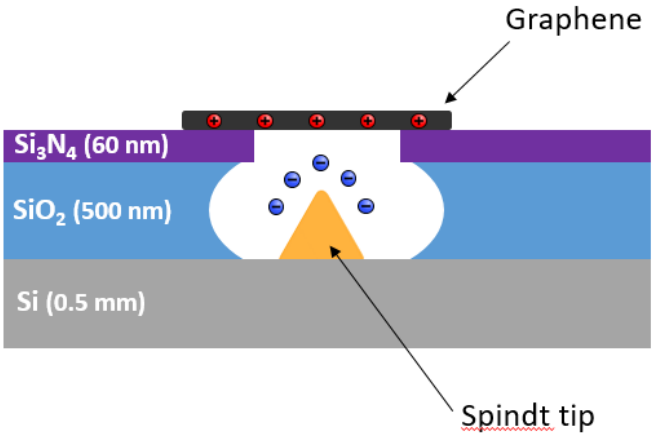

Figure 23. Schemtics of a 2D synthetic atom: A Spindt ridge in a trench

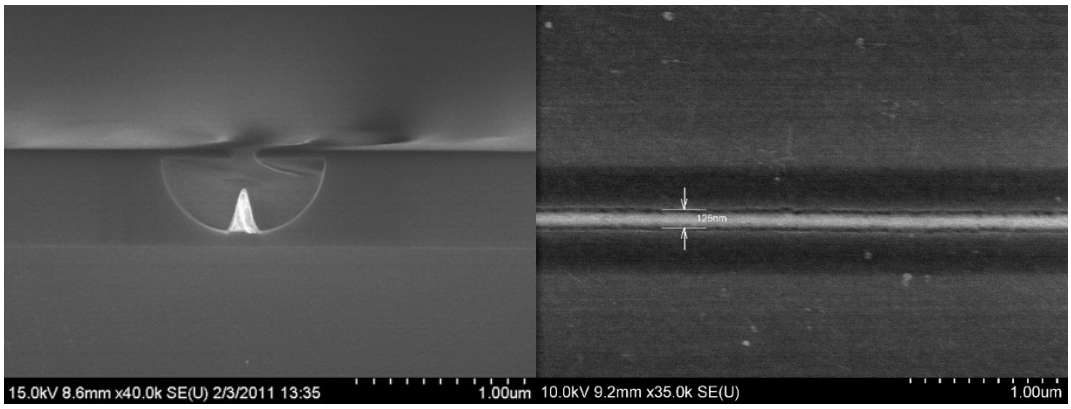

Figure 24. SEM images of a Spindt ridge in a trench (left) and the top view.

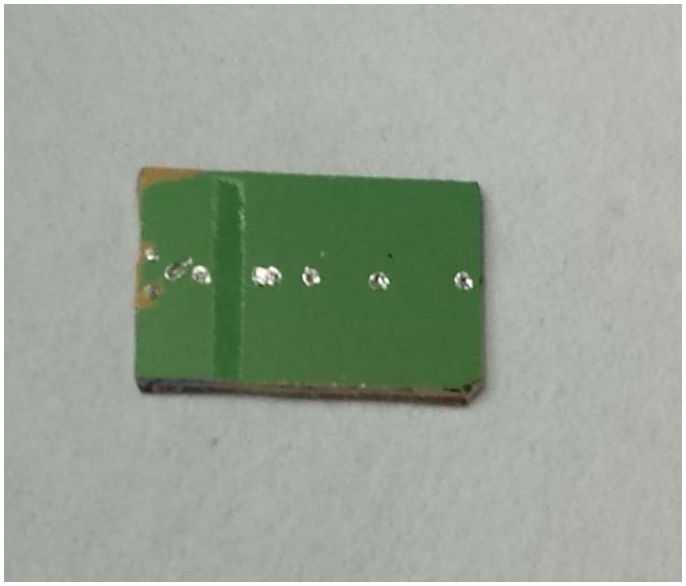

Figure 25. Picture of a Spindt ridge in a trench

Figure 26 is the top view the trench without and with the Gold Spindt ridge. The gold on the flat surface is eventually pulled off.

Figure 27 shows the device with a graphene layer.

Figure 28 shows typical I-V curves of the graphene nano capacitor at room temperature. The leak current is much smaller when the charge of the Spindt ridge is positive.

Figure 29 shows typical I-V curves of the graphene nano capacitor at 77K. The I-V curve is similar to the I-V curve at room temperature, but has more features. We are working on a theory.

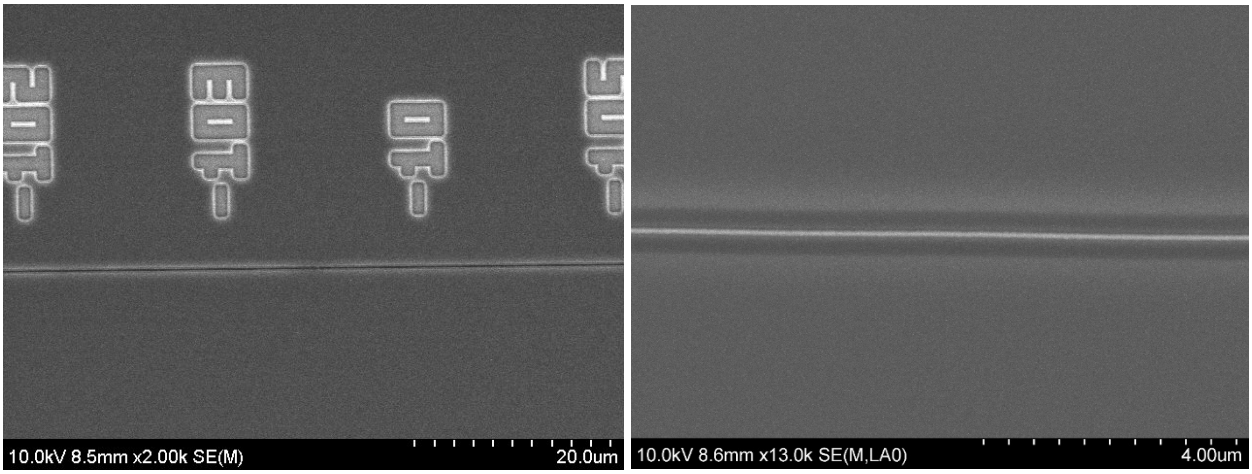

Figure 26. Trench before and after Au deposition.

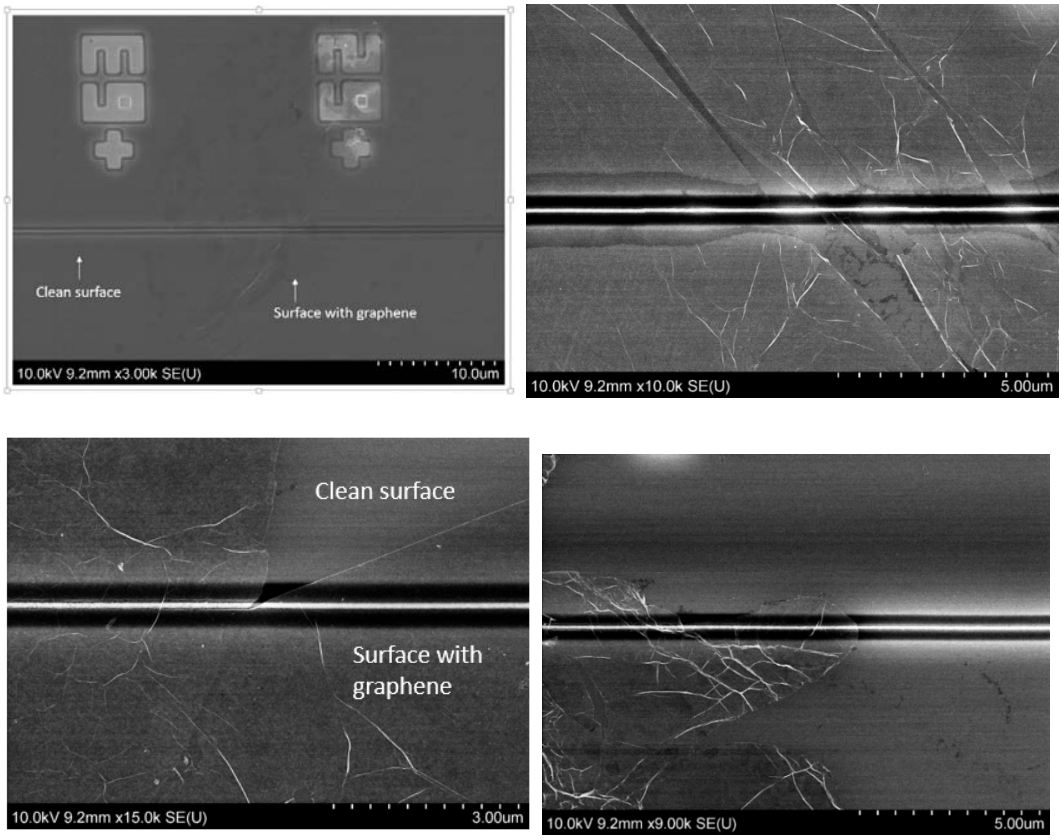

Figure 27. Sample images after graphene deposition

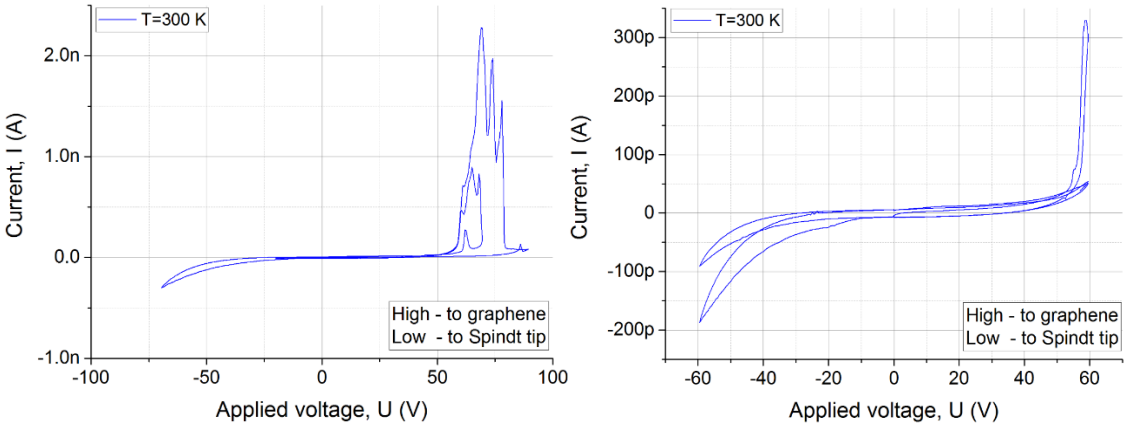

Figure 28. Current-Voltage characteristics at room temperature in air.

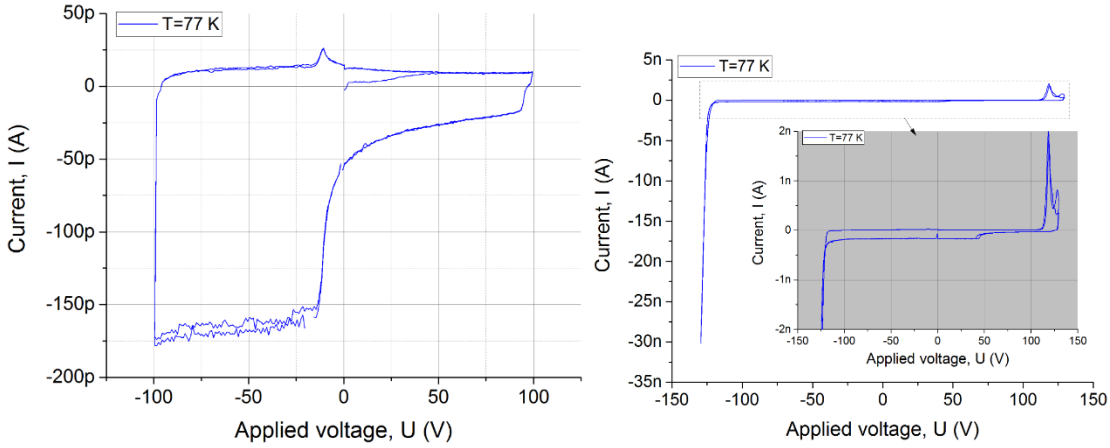

Figure 29. Current-Voltage characteristics at 77K.

Figure 30 shows damage done to the device due to break down. Figure 31 is a device with a discontinuous Spindt ridge due to a stitching problem with e-beam lithography.

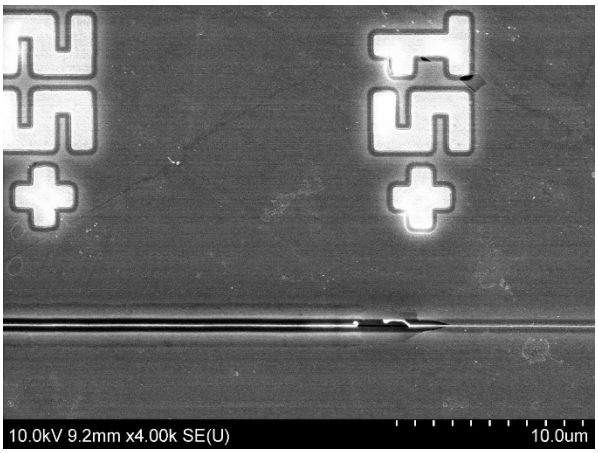

Figure 30. SEM image of the sample after local breakdown.

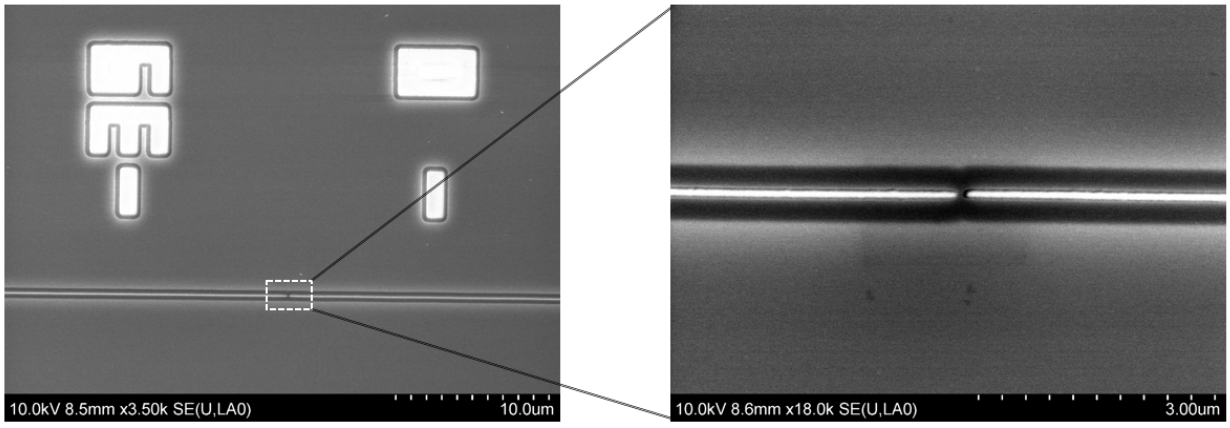

Figure 31. Bridges in trenches create interuptionds of the Spindt ridge.

In summary, the I-V curves (Current versus Voltage curves) at room temperature match expectation, but are more complex than expected at 77K.

Figure 32 shows attempts to control bridges in the trenches and other imperfections.

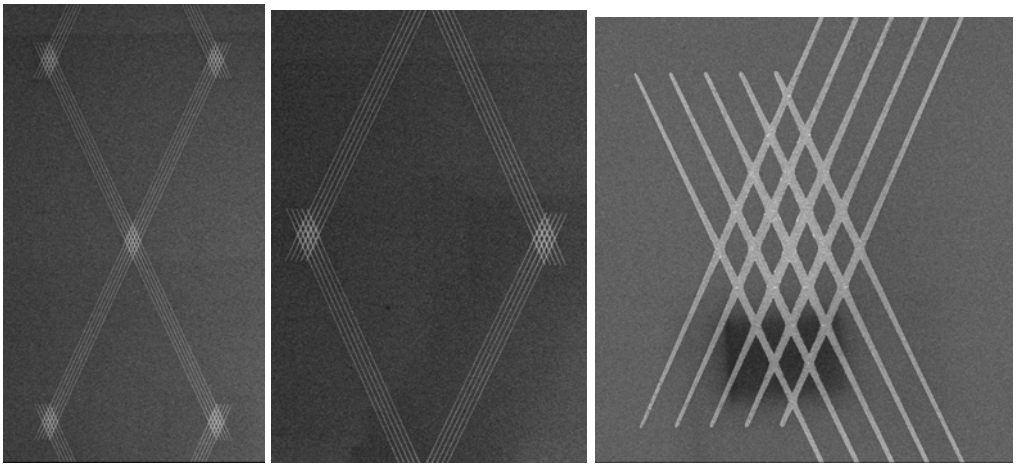

(a) (b) (c)

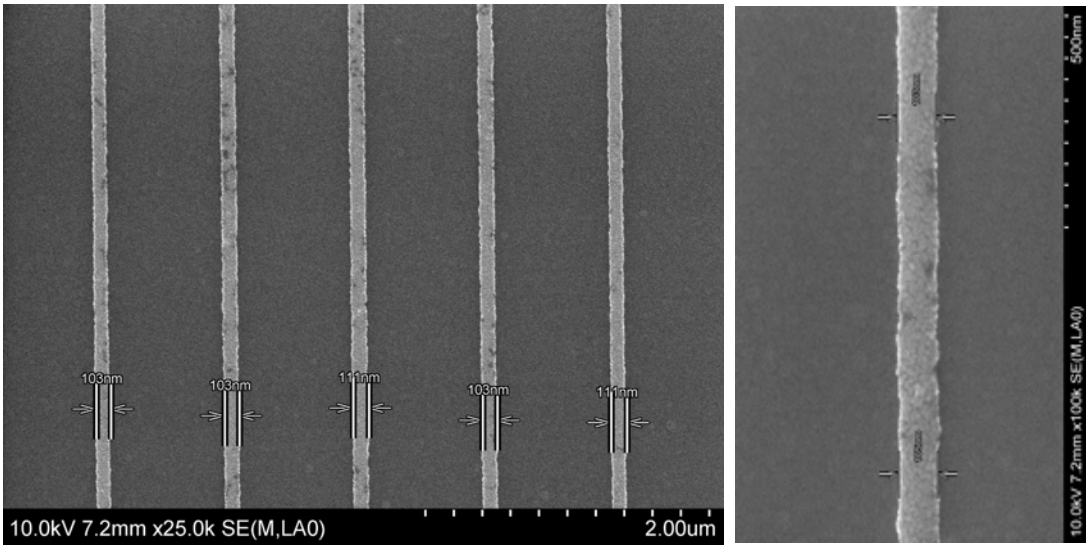

(d) (e)

Figure 32. Controlling bridges and stiching problems with angled arrays of trenches (a-e)

4.2.9. One-dimensional synthetic atom: A parallel plate vacuum nano-capacitor

We started to fabricate parallel plate vacuum nano-capacitors. Figure 33 shows the top view of nano-vacuum capacitors with SiO_2 spacers.

500 nm spacing

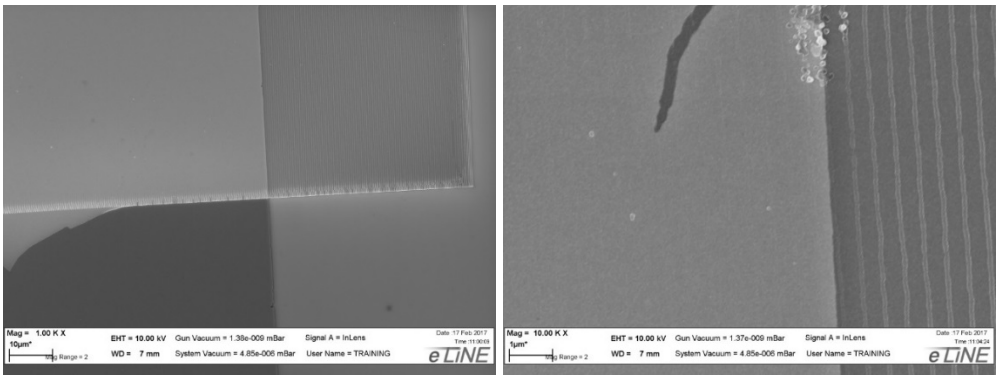

(a) (b)

1 um spacing

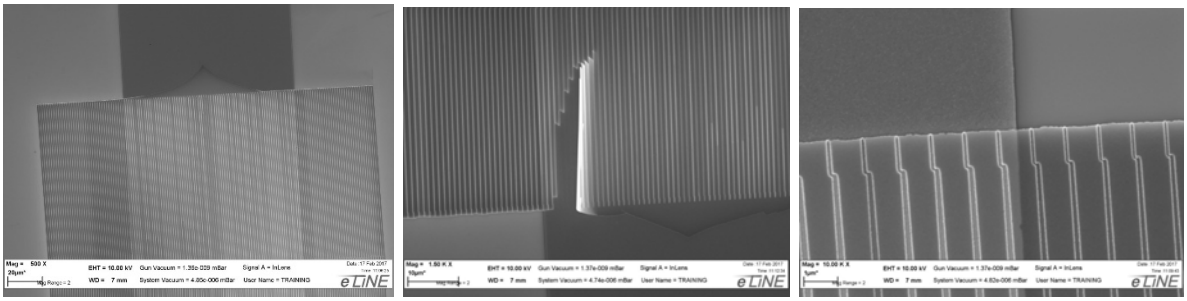

(c) (d) (e)

2 um spacing

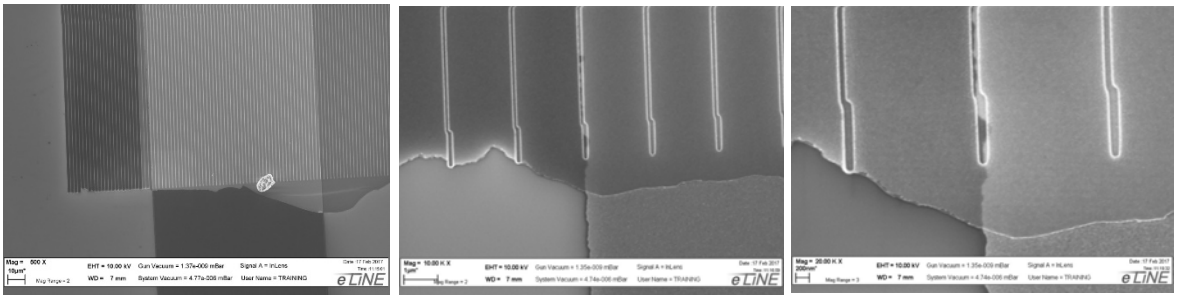

(f) (g) (h)

Figure 33. Fabrication of arrays one-dimensional synthetic atoms.

5. TASK III: INVESTIGATE RECOVERY OF ALUMINA NANOCAPACITORS AFTER HIGH-VOLTAGE BREAKDOWN

5.1. Methods, Assumptions, and Procedures

Previously we had discovered that Al_2O_3 nanocapacitors can self-repair [1]. Recently we discovered that our newly fabricated SiO_2 nanocapacitors can self-repair too. Figure 34 shows in red the applied voltage across a sample and a 10 MegaOhm resister in series. The blue curve is the sample resistance. This figure illustrates that SiO_2 nano-capacitors recover after breakdown.

Figure 34 shows the resistance versus time of a 113.5nm-thick SiO_2 nanocapacitor. This plot shows a breakdown on the first increase of voltage and shows that when the voltage was applied at 0.2V or -0.2V for an hour, the resistance increases. Since the resistance increases at low voltages after dielectric breakdown we can conclude that the dielectric recovers.

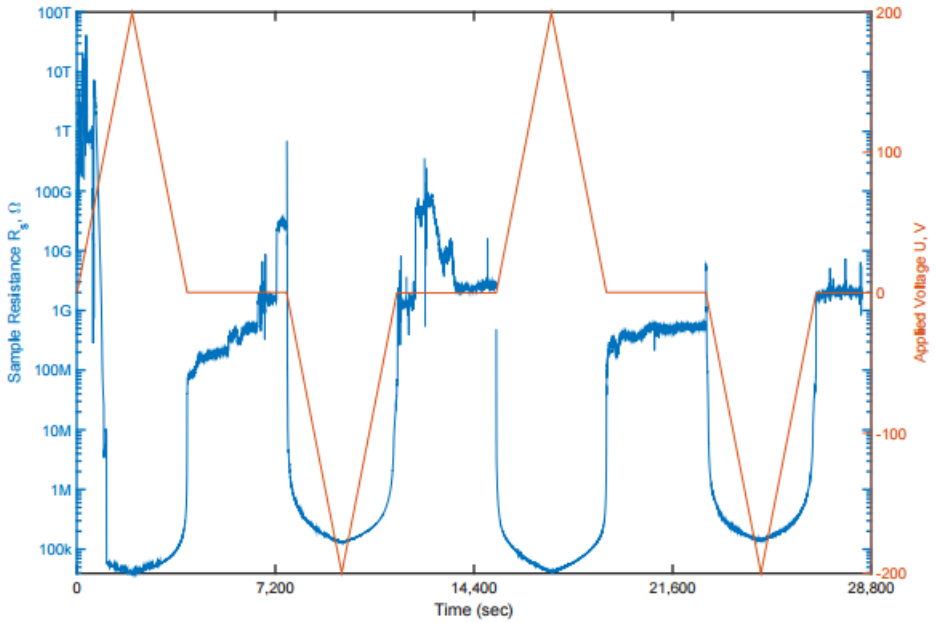

Figure 34. Plot of resistance on sample and applied voltage verses time

5.2. Results and Discussion

The recovery is on the minute-timescale. This suggests that it is a chemical process. We think that at breakdown the Aluminum electrode forms a thin wire from the cathode to the anode. If the wire has a diameter of less than 8 nm it will fully oxidize in the oxide rich environment of the dielectric layer within a few minutes. Therefore, the aluminum layer has to be in the 10 nm range. Otherwise the wire is thicker and does not fully oxidize after breakdown.

5.3. Conclusion

This means that nanocapacitors are self-repairing after breakdown, if the aluminum electrode has a thickness in the 10-nm range and the dielectric is in the 10-nm range.

We submitted a paper entitled “Recovery of alumina nanocapacitor after high-voltage breakdown” [11]. We filed a disclosure.

6. TASK IV: INVESTIGATE THE REDUCTION OF LEAK CURRENTS AND INCREASED DIELECTRIC STRENGTH DUE TO COULOMB BLOCKADE WILL BE STUDIED THEORETICALLY ON MULTI-DIMENSIONAL SYNTHETIC ATOMS

A 3-dimensional synthetic atom is a spherical capacitor on a nano-scale.

The electric field for a spherical capacitor is given by:

$$E(r) = \frac{Q}{4\pi\epsilon_0\epsilon_r r^2} \text{for} R_1 < r < R_2. \tag{8}$$

To solve the Schroedinger equation for a spherical capacitor, we make the following assumptions: We assume that there is only one electron in the capacitor that is we assume that there is no interaction between the electrons.

$$\left(-\frac{\hbar^2}{2m}\nabla^2 + V(\boldsymbol{r})\right)\Psi = E\Psi. \tag{9}$$

For a spherical capacitor the potential is given by

$$V(r) = \begin{cases} K_1 & r < R_1 \\ \frac{Qe}{4\pi\epsilon_0\epsilon_r}\left(\frac{1}{r} - \frac{1}{R_2}\right) & R_1 < r < R_2 \\ K_2 & R_2 < r < R_3 \\ 0 & R_2 < r \end{cases} \tag{10}$$

Where K_1 and K_2 are constants (related to the Fermi level) dependent on the material used. For now, we assume that the potential goes to zero, if r goes to infinity, where R_3 is the radius of the entire capacitor, including the outer shell. One can show that the momentum operator is independent of r. There on can separate the wave function into a spherical part and a radial part $\psi = R(r)Y(\Theta, \Phi)$. So we get for the Schroedinger equation:

$$-\frac{\hbar^2}{2m}\frac{1}{r}\partial_r^2(rRY) + \frac{L^2}{2mr^2}(RY) + V(r)RY = ERY \tag{11}$$

We can separate the spherical part $Y(\Theta, \Phi)$ and u(r)=r R(r)

$$-\frac{\hbar^2}{2m}u''(r) + V_{eff}(r)u(r) = Eu(r). \tag{12}$$

Where we use

$$V_{eff} = V(r) + \frac{l(l+1)\hbar^2}{2mr^2}. \tag{13}$$

Results with the values given: *E= 1 1V/nm* and *r=1nm*. We can use the formula for the electric field we get: $E = Q / (4\pi\varepsilon_0 r^2)$. Solving this equation for Q we get Q=1.11107x10-19C. For the distane between the first two energynlevels n=1 and n=2:

$$E_1 - E_2 = -\frac{R_y Q^2}{e^2}(1 - 1/4) = -4.91\text{eV} \tag{14}$$

For the value of kBT at room temperature T=298K we get

$$k_B T = 2.5710^{-2}\text{eV} \tag{15}$$

So, we see that quantization happens at room temperature because the value of $k_B T$ is a hundred times smaller than the distance between the first two energy levels.

The wave function for a hydrogen atom (which is the same for our simplified model if the charge in the center is Q = e) is given by [1]:

$$\psi_{n\ell m}(r, \vartheta, \varphi) = \sqrt{\left(\frac{2}{na_0}\right)^3 \frac{(n-\ell-1)!}{2n(n+\ell)!}} e^{-\rho/2} \rho^\ell L_{n-\ell-1}^{2\ell+1}(\rho) Y_\ell^m(\vartheta, \varphi) \tag{16}$$

ρ is given by $\rho = 2r / (n\, a_0)$. If we want to adjust this wave function for a center charge Q, we can use the definition of the Bohr raduis $a_0 = (4\pi\varepsilon_0 h^2) / (m_e e^2)$ and exchange one electron with the charge on the inner sphere. If $\hat{a}_0$ denotes the "Bohr radius" of the capacitor, we can write $\hat{a}_0 = a_0 Q/e$. This way we can easily adjust the wave function and any other problem for our case.

Now let us take a look at the degeneracy of the states. The quantum number l is defined as $0 \leq l \leq$ n-1 and the quantum number is defined by $0 \leq |m| \leq l$. Therefore we have for each l-value 2l+1 degenerate states and for each n we have:

$$\sum_{l=0}^{n-1} 2l + 1 = n^2 \tag{17}$$

degenerate states. If we assume that the wave function behaves as the wave funtion for a hydrogen, we can calculate the number of electrons if all states are occupied. We can put two electrons in each state due to Pauli's exclusion principle, For the radius of one orbital we use the following formula:

$$r = n^2 \tilde{a_0} = n^2 \frac{a_0 e}{Q} \tag{18}$$

So we get for the first orbital inside the capacitor $r=R_1$ and the last one that is inside the capacitor $r = R_n$:

$$\begin{aligned} R_1 &= n_1^2 \frac{a_0 e}{Q} \\ R_2 &= n_2^2 \frac{a_0 e}{Q} \end{aligned} \tag{19}$$

So we get for the number of electrons in the capacitor:

$$N_e = 2 \times \sum_{n=n_1}^{n_2} n^2 = \frac{2}{3}(n_2^3 - n_1^3) + (n_2^2 + n_1^2) + \frac{1}{3}(n_2 - n_1) \tag{20}$$

We know that n_i is proportional to $(R_i)^{1/2}$ (we assume that we get integer values), we can now compare this quantity to the volume of the capacitor $V = 4/3\ \pi(R_2^3 - R_1^3)$.

We can calculate the transition rate between two states using:

$$A = \frac{\omega^3 d^2}{3\pi\varepsilon_0 \hbar c^3} \tag{21}$$

Ω denotes the emission frequency, $d=e^2|\langle 1|r|2\rangle|^2$ is the mean squared average of the electric dipole moment [2][3]. The emission frequency is given by $\hbar\omega = E_{n2} - E_{n1}$. Using these results we can now, for example, calculate the transition rate for 2P $\leftarrow$2S. To get the dipole moment, we implemented the wave functions in Mathematica. Additionally we compted the trasition rates for $\langle 1|r_i|2\rangle$.

We calculated the transition rate for 5P $\rightarrow$4S, because the n=4 orbital is the first that is actually inside the capacitor. So this is between the two lowest states of the capacitor. The transition rate is independent of m, we used m=0. For the calculations we used for the charge of the inner sphere Q = e, but the calculations could be easily redone for a different charge:

$$\begin{aligned} &\langle 4,0,0|x|5,1,0\rangle = 0 \\ &\langle 4,0,0|y|5,1,0\rangle = 0 \\ &\langle 4,0,0|z|5,1,0\rangle = 4.918\, a_0 \\ &d^2 = e^2 a_0^2 \times 24.185 \end{aligned} \tag{22}$$

And we get for the emission frequency:

$$\begin{aligned} E_4 &= -0.85\text{eV} \\ E_5 &= -0.544\text{eV} \\ \Delta E = E_5 - E_4 &= \hbar\omega \Leftrightarrow \omega = 4.65 \times 10^{14}\,\text{s}^{-1}. \end{aligned} \tag{23}$$

And finally get for the transition rate:

$$A_{5P\to 4S} = \frac{\omega^3 d^2}{3\pi\varepsilon_0 \hbar c^3} = 7.37 \times 10^5\,\text{s}^{-1}. \tag{24}$$

The quantum capacitance for a spherical quantum dot is given by:

$$C_Q(N) = \frac{e^2}{E(N+1) - 2E(N) + E(N-1)}. \tag{25}$$

The quantum capacitance depends on the occupied states. N is is the Nth particle of the system. E(N) is the energy of that particle [6]. The theoretical model that describes quantum is given below. [7]:

$$\mu(N) = E(N) - E(N-1). \tag{26}$$

The chemical potential describes the energy, which we need to add to one electron.

$$\begin{aligned} &\frac{1}{C} = \frac{\Delta V}{\Delta Q} \\ &\Delta V = \frac{\Delta\mu}{e} = \frac{\mu(N+\Delta N) - \mu(N)}{e} \\ &\text{We set } \Delta N = 1 \\ &\Rightarrow C_Q(N) = \frac{e^2}{\mu(N+1) - \mu(N)} = \frac{e^2}{E(N+1) - 2E(N) + E(N-1)}. \end{aligned} \tag{27}$$

These calculation suggest that the leakage current at room temperature is very small in a spherical nanocapacitor due to Coulomb blockade.

7. CONCLUSIONS

From a research perspective, the largest achievement of this project was that Coulomb blockade describes the behavior of the charge, i.e. there are space charges inside the dielectric which need to tunnel through a surface barrier and surface charges which leave the surface on a time scale given by the external resistor and the capacity of the capacitor. In our nanocapacitors, the time scale of the space charges is much larger than the time scale of the surface charges.

From a practical perspective, the most important finding is that there seem to be no obstacles in fabricating stacks of nanocapacitors with many layers.

REFERENCES

1. Lyon D., Hubler A., "Gap size dependence of the dielectric strength in nano vacuum gaps," *IEEE Trans. Dielectr. Electr. Insul.* **20**, pp. 1467-1471, 2013.

2. Hubler A., Osuagwu O., "Digital quantum batteries: energy and information storage in nanovacuum tube arrays," *Complexity* **15**, pp. 48-55, 2010.

3. White H.J., "Absorption current, dielectric constant and dielectric loss by the tunneling mechanism," *J. App. Phys.*, **44**(6), 1973.

4. Gross B., "On permanent charges in solid dielectrics," *J. Chem. Phys*., **11**(10), pp. 866-872, 1949.

5. Gupta H., Singh K., John T., "Analysis of dielectric absorption in capacitors," *JAIR*, **3**(6), pp. 255-257, 2014.

6. Das-Gupta D.K., "Conduction mechanisms and high-field effects in synthetic insulating polymers," *IEEE Trans. Dielectr. Electr. Insul.*, **4**(2), pp. 149-156, 1997.

7. Lowell J., "Tunneling between metals and insulators and its role in contact electrification," *J. Phys.* D, **12**, pp. 1541-1554, 1979.

8. Garton C.G., "Charge transfer from metal to dielectric by contact potential," *J. Phys. D*, **7,** 1974.

9. Jonscher A., "Dielectric relaxation in solids," *J.Phys. D*, **32** R57, 1999.

10. Ricco B., Azbel M., Ya., and Brodsky M.H., "Novel Mechanism for Tunneling and Breakdown of Thin Si02 Films," *Phys. Rev. Lett.* **51**, 1983.

11. Belkin A., Bezryadin A., Hendren L., and Hubler A., "Recovery of alumina nanocapacitors after high-voltage breakdown," *Scientific Reports* **7**, Article number: 932, 2017.

LIST OF SYMBOLS, ABBREVIATIONS, AND ACRONYMS

Al	Aluminum
Al_2O_3	Aluminium oxide, Alumina
ALD system	Atomic Layer Depositon system
CFE	Cold Field Emission
I-V curve	A graph of the current I versus the voltage V
ODE	Ordinary Differential Equation
RC	Resistance-Capacitance
RF	Radio Frequency
SEM image	Scanning Electron Microscope
SiO_2	Silicon dioxide

DISTRIBUTION LIST

DTIC/OCP
8725 John J. Kingman Rd, Suite 0944
Ft Belvoir, VA 22060-6218 1 cy

AFRL/RVIL
Kirtland AFB, NM 87117-5776 1 cy

Official Record Copy
AFRL/RVSV/Jessica Buckner 1 cy